Vol 15 No 8, August 2006
1009-1963/2006/15(08)/1824-07
Chinese Physics
© 2006 Chin. Phys. Soc.
and IOP Publishing Ltd

Full-vectorial finite-difference beam propagation method based on the modified alternating direction implicit method

Xiao Jin-Biao(肖金标)† and Sun Xiao-Han(孙小菡)

Laboratory of Photonics and Optical Communications, Department of Electronic Engineering, Southeast University, Nanjing 210096, *China*

(Received 9 November 2005; revised manuscript received 26 February 2006)

A modified alternating direction implicit algorithm is proposed to solve the full-vectorial finite-difference beam propagation method formulation based on H fields. The cross-coupling terms are neglected in the first sub-step, but evaluated and doubly used in the second sub-step. The order of two sub-steps is reversed for each transverse magnetic field component so that the cross-coupling terms are always expressed in implicit form, thus the calculation is very efficient and stable. Moreover, an improved six-point finite-difference scheme with high accuracy independent of specific structures of waveguide is also constructed to approximate the cross-coupling terms along the transverse directions. The imaginary-distance procedure is used to assess the validity and utility of the present method. The field patterns and the normalized propagation constants of the fundamental mode for a buried rectangular waveguide and a rib waveguide are presented. Solutions are in excellent agreement with the benchmark results from the modal transverse resonance method.

Keywords: beam propagation method, alternating direction implicit algorithm, finite difference, optical waveguides, integrated optics

PACC: 4280L, 4280S, 4282, 4110H

1. Introduction

The beam propagation method (BPM) has become one of the most popular and powerful numerical techniques for modelling electromagnetic wave propagation in photonic devices.[1−4] There are three main BPM approaches currently available: scalar,[5,6] semi-vectorial,[7,8] and full-vectorial formalisms.[9−11] For complicated photonic devices in which large refractive index contrasts and/or polarization effects are involved, three-dimensional full-vectorial BPM (3D-FV-BPM) is needed.[1,2] Over the years, various versions of 3D-FV-BPM have been proposed and successfully applied to solve either the optical field propagation problems or the guided-modes for optical waveguides.[1,2] Among them, the 3D-FV-BPM based on finite difference (FD) method (3D-FV-FDBPM) is attractive due to the simplicity of its implementation and the sparsity of its resulting matrix.[9−11]

The discretization for 3D-FV-BPM formulation along the longitudinal direction (z-direction) and transverse directions (x- and y-directions) should be dealt with carefully in order to improve the efficiency and/or accuracy with stability. For discretization along the longitudinal direction, pioneering work has been done by Huang and Xu[9] by using an iterative solver, which is somewhat time-consuming because of the iterative nature. Instead, the alternating direction implicit (ADI) algorithm is a non-iterative procedure for solving multidimensional partial differential equations,[12] so the calculation is efficient and it does not suffer from non-convergence. The ADI method via the Crank–Nicholson (CN) scheme was first proposed by Yamauchi *et al* [13] to solve the 3D scalar BPM formulation, and same algorithm was also used by Liu *et al* [14] to solve the semi-vectorial BPM formulation. More recently, the ADI method via CN scheme was used by Hseuh *et al* [10] to solve the full-vectorial BPM formulation. However, Rao[15] has proved that it is not numerically unconditionally stable when the ADI method via CN scheme is applied to the 3D-FV-BPM. Therefore, the introduction of new algorithms is still under investigation. On the other hand, for discretization along the transverse directions, the ac-

†Corresponding authors, E-mail: jbxiao@seu.edu.cn

curacy of 3D-FV-BPM strongly depends on the FD scheme for the cross-coupling terms (CCTs). A direct discretization for the CCTs has been proved to result in poor convergence behaviour.[9] So, new FD scheme should be also proposed for improving the computational accuracy. Moreover, although all field components can be calculated from either transverse electrical (E-formulation) or magnetic formulation (H-formulation), the resulting fields do not always look exactly the same.[2] In addition, the derivatives of magnetic field components h_x and h_y at horizontal and vertical interfaces, respectively, are discontinuous. Therefore, as a general rule, if magnetic field components are desired, it is best to choose the H-formulation.

In this paper, a modified ADI algorithm is proposed for discretizing the 3D-FV-BPM formulation based on H fields along the longitudinal direction. In the first sub-step, the field propagates in the absence of the CCTs, and then they are doubly used in second sub-step. The order of two sub-steps is reversed for each transverse magnetic field component so that the CCTs are always treated implicitly. Therefore, the calculation is very efficient and stable. Moreover, an improved six-point FD scheme with high accuracy is also developed to approximate the CCTs along the transverse directions, which takes into account the discontinuities of the derivatives of magnetic field components h_x and h_y at horizontal and vertical interfaces respectively, and is independent of specific structures of waveguide. In addition, if the field propagates along the imaginary axis (imaginary-distance BPM), the corresponding procedure is efficient to solve the guided-modes for optical waveguides.[16,17] Therefore, we use the imaginary-distance procedure to assess the validity and utility of the present technique.

2. Description of the method

2.1. Basic formulation for 3D-FV-BPM based on H fields

The vectorial wave equation based on H fields is directly derived from Maxwell's equations and it is given as follows:

$$\nabla^2 \boldsymbol{H} + \frac{1}{n^2}\left(\nabla n^2\right) \times (\nabla \times \boldsymbol{H}) + k_0^2 n^2 \boldsymbol{H} = 0, \quad (1)$$

where $k_0 = \omega\sqrt{\varepsilon_0 \mu_0}$ is the wavenumber in free space and $n = n(x,\ y,\ z)$ is the refractive index of the medium. If the refractive index varies slowly along the direction of the wave propagation (say, z-direction), the transverse components in Eq.(1) can be approximated by

$$\nabla^2 H_x + k_0^2 n^2 H_x - \frac{1}{n^2}\frac{\partial n^2}{\partial y}\left(\frac{\partial H_x}{\partial y} - \frac{\partial H_y}{\partial x}\right) = 0, \quad (2a)$$

$$\nabla^2 H_y + k_0^2 n^2 H_y - \frac{1}{n^2}\frac{\partial n^2}{\partial x}\left(\frac{\partial H_y}{\partial x} - \frac{\partial H_x}{\partial y}\right) = 0. \quad (2b)$$

Using the slowly-varying envelope approximation, we get

$$H_x = h_x \exp(-\mathrm{j}k_0 n_0 z), \quad (3a)$$

$$H_y = h_y \exp(-\mathrm{j}k_0 n_0 z), \quad (3b)$$

where n_0 is the reference index. Substituting Eq.(3) into Eq.(2), and neglecting the terms of the second derivatives with respective to z, we can reduce Eq.(2) to

$$\frac{\partial h_x}{\partial z} = \left(A_{xx}^x + A_{xx}^y\right) h_x + A_{xy} h_y, \quad (4a)$$

$$\frac{\partial h_y}{\partial z} = \left(A_{yy}^x + A_{yy}^y\right) h_y + A_{yx} h_x \quad (4b)$$

with

$$A_{xx}^x h_x = \frac{-\mathrm{j}}{2k_0 n_0}\left\{\frac{\partial^2 h_x}{\partial x^2} + \frac{1}{2}k_0^2\left(n^2 - n_0^2\right) h_x\right\}, \quad (5a)$$

$$A_{xx}^y h_x = \frac{-\mathrm{j}}{2k_0 n_0}\left\{n^2\left[\frac{\partial}{\partial y}\left(\frac{1}{n^2}\frac{\partial h_x}{\partial y}\right)\right] + \frac{1}{2}k_0^2\left(n^2 - n_0^2\right) h_x\right\}, \quad (5b)$$

$$A_{yy}^x h_y = \frac{-\mathrm{j}}{2k_0 n_0}\left\{n^2\left[\frac{\partial}{\partial x}\left(\frac{1}{n^2}\frac{\partial h_y}{\partial x}\right)\right] + \frac{1}{2}k_0^2\left(n^2 - n_0^2\right) h_y\right\}, \quad (5c)$$

$$A_{yy}^y h_y = \frac{-\mathrm{j}}{2k_0 n_0}\left\{\frac{\partial^2 h_y}{\partial y^2} + \frac{1}{2}k_0^2\left(n^2 - n_0^2\right) h_y\right\}, \quad (5d)$$

$$A_{xy} h_y = \frac{-\mathrm{j}}{2k_0 n_0}\left\{\frac{\partial^2 h_y}{\partial y \partial x} - n^2\left[\frac{\partial}{\partial y}\left(\frac{1}{n^2}\frac{\partial h_y}{\partial x}\right)\right]\right\}, \quad (5e)$$

$$A_{yx} h_x = \frac{-\mathrm{j}}{2k_0 n_0}\left\{\frac{\partial^2 h_x}{\partial x \partial y} - n^2\left[\frac{\partial}{\partial x}\left(\frac{1}{n^2}\frac{\partial h_x}{\partial y}\right)\right]\right\}. \quad (5f)$$

Eq.(4) together with Eq.(5) is the basic formulation for 3D-FV-BPM based on H fields.

2.2. The discretization along the longitudinal direction

We first discretize the Eq.(4) along the longitudinal direction. A modified ADI algorithm is proposed to perform this task. The algorithm is summarized as follows:

1) First sub-step: $z = l\Delta z \rightarrow z = \left(l + \frac{1}{2}\right)\Delta z$

$$\left(1 - \frac{\Delta z}{2}A^x_{xx}\right) h_x\left(p, q, l + \frac{1}{2}\right) = \left(1 + \frac{\Delta z}{2}A^y_{xx}\right) h_x(p, q, l), \tag{6a}$$

$$\left(1 - \frac{\Delta z}{2}A^x_{yy}\right) h_y(p, q, l + \frac{1}{2}) = \left(1 + \frac{\Delta z}{2}A^y_{yy}\right) h_y(p, q, l) + \Delta z \left[A_{yx}h_x(p, q, l + \frac{1}{2})\right]. \tag{6b}$$

2) Second sub-step:$z = \left(l + \frac{1}{2}\right)\Delta z \rightarrow z = (l + 1)\Delta z$

$$\left(1 - \frac{\Delta z}{2}A^y_{yy}\right) h_x(p, q, l + 1) = \left(1 + \frac{\Delta z}{2}A^x_{xx}\right) h_x\left(p, q, l + \frac{1}{2}\right), \tag{6c}$$

$$\left(1 - \frac{\Delta z}{2}A^y_{xx}\right) h_x(p, q, l + 1) = \left(1 + \frac{\Delta z}{2}A^x_{xx}\right) h_x\left(p, q, l + \frac{1}{2}\right) + \Delta z \left[A_{xy}h_y(p, q, l + 1)\right], \tag{6d}$$

where $h_x(p, q, l)$, $h_x\left(p, q, l + \frac{1}{2}\right)$, and $h_x(p, q, l + 1)$ denote the component of h_x at plane $z = l\Delta z$, z=$(l$+1/2$)\Delta z$, and z=$(l$+1$)$ with $x = p\Delta x$ and $y = q\Delta y$ respectively, $\Delta x \times \Delta y$ is the mesh size in transverse directions, and Δz is the propagation step. The same notation is also used for h_y. In present algorithm, the propagation step $z = l\Delta z \rightarrow z = (l + 1)\Delta z$ is split into two sub-steps $z = l\Delta z \rightarrow z = \left(l + \frac{1}{2}\right)\Delta z$ and $z = \left(l + \frac{1}{2}\right)\Delta z \rightarrow z = (l + 1)\Delta z$. In the first sub-step, the field propagates in the absence of the CCTs, e.g. Eq.(6a), and then they are evaluated and doubly used in the second sub-step, e.g. Eq.(6d). The order of the two sub-steps is reversed for each magnetic field component so that the CCTs are always expressed in implicit form, that is, Eq.(6a) and Eq.(6d) for h_x, and Eq.(6b) and Eq.(6c) for h_y. The resulting matrix is tridiagonal, so the calculation is very efficient and stable. Moreover, thanks to the ADI method the present algorithm does not suffer from non-convergence.

2.3. The discretizations along the transverse directions

Next, we discretize Eq.(4) along the transverse directions. If the CCTs in Eq.(4) are neglected, 3D semi-vectorial BPM formulations are obtained, so the discretizations for $A^x_{xx}h_x$,$A^y_{xx}h_x$, $A^x_{yy}h_y$, and $A^y_{yy}h_y$ are the same as those used in Ref.[9]. As mentioned above, the accuracy is severely restricted by the FD scheme for the CCTs along the transverse directions which are indispensable in a 3D-FV-BPM. Here, we propose an improved scheme for approximating the CCTs:

$$\begin{aligned}
A_{xy}h_y\big|_{p.q,l} =& \frac{-\mathrm{j}}{8k_0n_0\Delta x\Delta y}\left\{\left[1 - \frac{2n^2(p+1,q,l)}{n^2(p+1,q,l) + n^2(p+1,q+1,l)}\right] h_y(p+1,q+1,l)\right.\\
&- \left[1 - \frac{2n^2(p+1,q,l)}{n^2(p+1,q,l) + n^2(p+1,q-1,l)}\right] h_y(p+1,q-1,l)\\
&- \left[1 - \frac{2n^2(p-1,q,l)}{n^2(p-1,q,l) + n^2(p-1,q+1,l)}\right] h_y(p-1,q+1,l)\\
&+ \left[1 - \frac{2n^2(p-1,q,l)}{n^2(p-1,q,l) + n^2(p-1,q-1,l)}\right] h_y(p-1,q-1,l)\\
&+ \left[\frac{2n^2(p+1,q,l)}{n^2(p+1,q,l) + n^2(p+1,q+1,l)} - \frac{2n^2(p+1,q,l)}{n^2(p+1,q,l) + n^2(p+1,q-1,l)}\right] h_y(p+1,q,l)\\
&- \left.\left[\frac{2n^2(p-1,q,l)}{n^2(p-1,q,l) + n^2(p-1,q+1,l)} - \frac{2n^2(p-1,q,l)}{n^2(p-1,q,l) + n^2(p-1,q-1,l)}\right] h_y(p-1,q,l)\right\}.
\end{aligned} \tag{7}$$

The present formula is a six-point FD scheme, which takes into account the discontinuities of the derivatives of magnetic field components at horizontal and vertical interfaces respectively, and is independent of specific structures of waveguide. So, the computational accuracy of our scheme is much higher than that of four-point FD scheme from the direct discretization and the procedure is simple and versatile. For boundaries of the computational window, the transparent boundary condition[18] is used in our algorithm in order to eliminate the non-physical reflection.

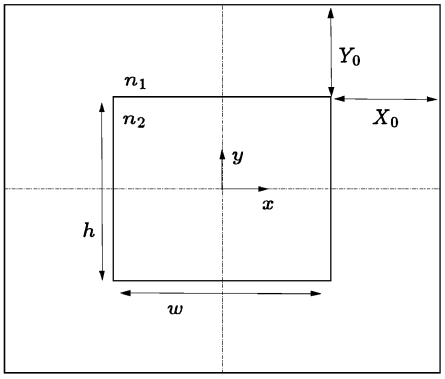


Fig.1. Geometry of a buried rectangular waveguide.

3. Numerical results

Firstly we calculate the normalized propagation constants and the patterns of the fundamental mode for a typical buried rectangular waveguide whose geometry is shown in Fig.1, in which $w = h$=1.0μm, n_1=1.0, n_2=1.5, and $X_0 = Y_0$=2.0μm at wavelength λ=1.5μm.

The fundamental mode can be calculated by the imaginary-distance procedure in which the coordinate z in the propagation direction is changed to $j\tau$.[16,17] The effective index n_{eff} is evaluated by the growth in the field amplitude

$$n_{\text{eff}}(\tau) = n_0 + \frac{\ln\left\{\int \phi(x,y,\tau+\Delta\tau)\mathrm{d}x\mathrm{d}y\right\} - \ln\left\{\int \phi(x,y,\tau)\mathrm{d}x\mathrm{d}y\right\}}{k_0\Delta\tau}, \tag{8}$$

and the normalized propagation constant B is here defined as

$$B = \frac{n_{\text{eff}}^2 - n_1^2}{n_2^2 - n_1^2}. \tag{9}$$

As the injected field, we chose a step function as

$$\phi(x,y,0) = \begin{cases} 1, \text{ for } \ |x| \le 0.5\mu\text{m} \ \text{ and } |y| \le 0.5\mu\text{m} \\ 0, \text{ otherwise} \end{cases} \tag{10}$$

for the major component and zero for the minor component. The reference index is $n_0 = (n_1 + n_2)/2$.

Figure 2 shows that the normalized propagation constants B for the fundamental mode as a function of propagation τ. The propagation step size is fixed at $\Delta\tau$=0.1μm and the transverse mesh size is chosen as $\Delta x = \Delta y$=0.025μm. It can be seen that the convergence values of the normalized propagation constants for both Quasi-TE mode and Quasi-TM mode are obtained after propagation only 10μm. The value for the Quasi-TE mode is identical to that for the Quasi-TM at each propagation step. In addition, the solutions keep convergence after we propagate the injected fields till 50μm, thus the calculation is stable. Moreover, the resulting equation systems are solved by using MATLAB subroutines and implemented on a Pentium IV CPU PC with a CPU clock of 2.0GHz. It is found that the required CPU time for one propagation step is less than 1 second (the number of transverse mesh points is 100×100). The computational time for the same problem by using iterative solver in Ref.[9] is over 10 seconds. Therefore, the present method is very efficient. The convergence value is B=0.4907. Our solution is very close to the value (B=0.4904) from the modal transverse resonance method (MTRM),[19] which is so far regarded as a benchmark result for comparison of accuracy.

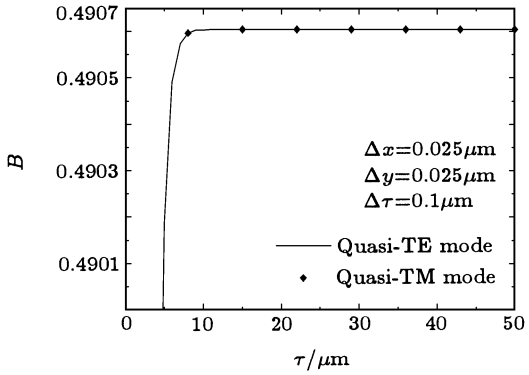


Fig.2. Normalized propagation constants B for the fundamental mode as a function of propagation τ.

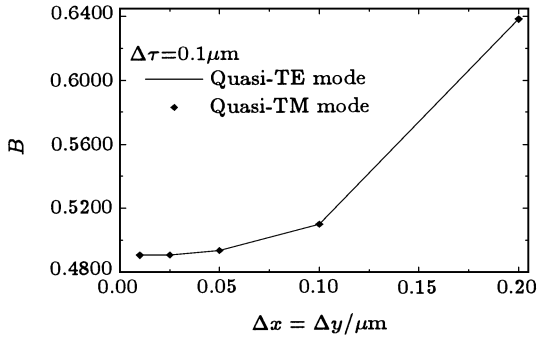


Fig.3. Normalized propagation constants B for the fundamental mode as a function of transverse mesh size $\Delta x = \Delta y$.

We also investigate the convergence of the normalized propagation constants as functions of the transverse mesh size and longitudinal step size. Figure 3 plots the results of the calculation as a function of the transverse mesh size $\Delta x = \Delta y$ with the propagation step size $\Delta\tau$=0.1μm. It is apparent that the solutions converge to the values from MTRM as the transverse mesh size decreases. Therefore, the numerical dispersion is reduced with the decrease of the transverse mesh size. Figure 4 gives the solutions of the calculation as a function of propagation step size $\Delta\tau$ with the transverse mesh size $\Delta x = \Delta y$ =0.025μm. It is noted that the variation of the propagation size does not have much influence on the accuracy of the normalized propagation constants, so relatively large propagation step size $\Delta\tau$ may be used in present method.

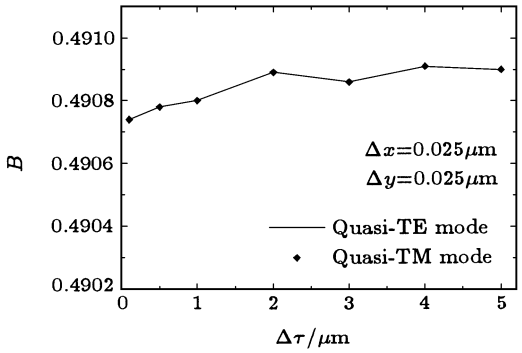


Fig.4. Normalized propagation constants B for the fundamental mode as a function of propagation step size $\Delta\tau$.

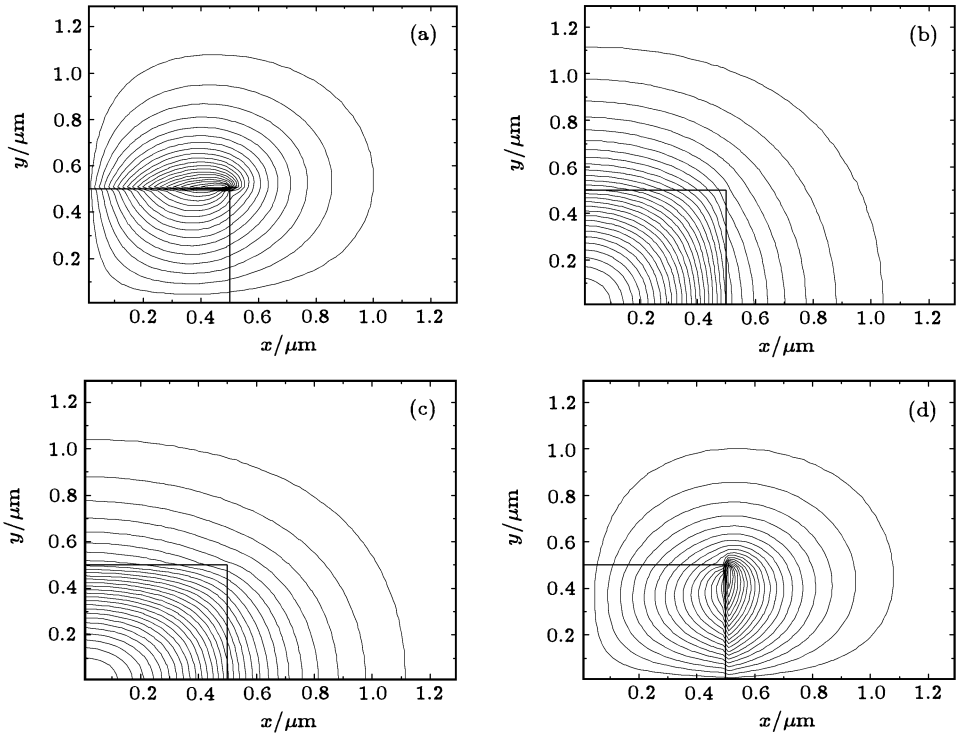


Fig.5. Field patterns of the fundamental mode for a buried rectangular waveguide: Quasi-TE mode (a) h_x and (b) h_y; Quasi-TM mode (c) h_x and (d) h_y.

Figure 5 illustrates the typical field patterns for the fundamental mode in quasi-TE and quasi-TM modes. Only one-quarter of the field profiled are displayed because of the symmetric structure of the waveguide. It is seen that a single peak appears in the guiding region for the major component, and four peaks locate at the corners for the minor component. In addition, the discontinuous feature of the derivatives of magnetic field components h_x and h_y at horizontal and vertical interfaces, respectively, are clearly observed. So, the hybrid nature of the full-vectorial guided-modes is successfully demonstrated.

The second example is a rib waveguide as shown in Fig.6. The refractive indices of the cover, core, and substrate are n_1=1.0, n_2=3.44, and n_3=3.40 respectively. The height and the width of the rib are h=1.0μm and w=3.0μm respectively. The thickness of the slab waveguide is t=0.5μm at wavelength λ=1.15μm. The computational window parameters are Y_a=0.5μm above the top of the rib, Y_b=3.0μm below the guiding layer, and X_a=2.5μm aside from the rib lateral side. The transverse mesh size is $\Delta x = \Delta y$=0.025μm, and the propagation step is Δz=0.1μm. Table 1 shows normalized propagation constants of the fundamental mode for Quasi-TE and Quasi-TM after the propagation reaches the convergence. In order to examine the accuracy of the present method, the results of the analysis under study together with those of 3D-FV-FDBPM with traditional FD scheme for the CCTs,[9] full-vectorial finite-difference method (FV-FD),[20] mapped Galerkin method (MGM)[21] and

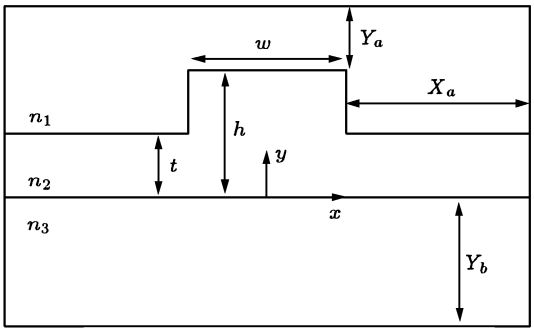


Fig.6. Geometry of a rib waveguide.

Table 1. Normalized propagation constant for a rib waveguide computed by different methods.

method	Quasi-TE mode	Quasi-TM mode
FV-FD[20]	0.3301	0.2912
3D-FV-FDBPM[9]	0.3303	0.2915
MGM[21]	0.3246	0.2880
NTRM[19]	0.3270	0.2890
Present results	0.3274	0.2892

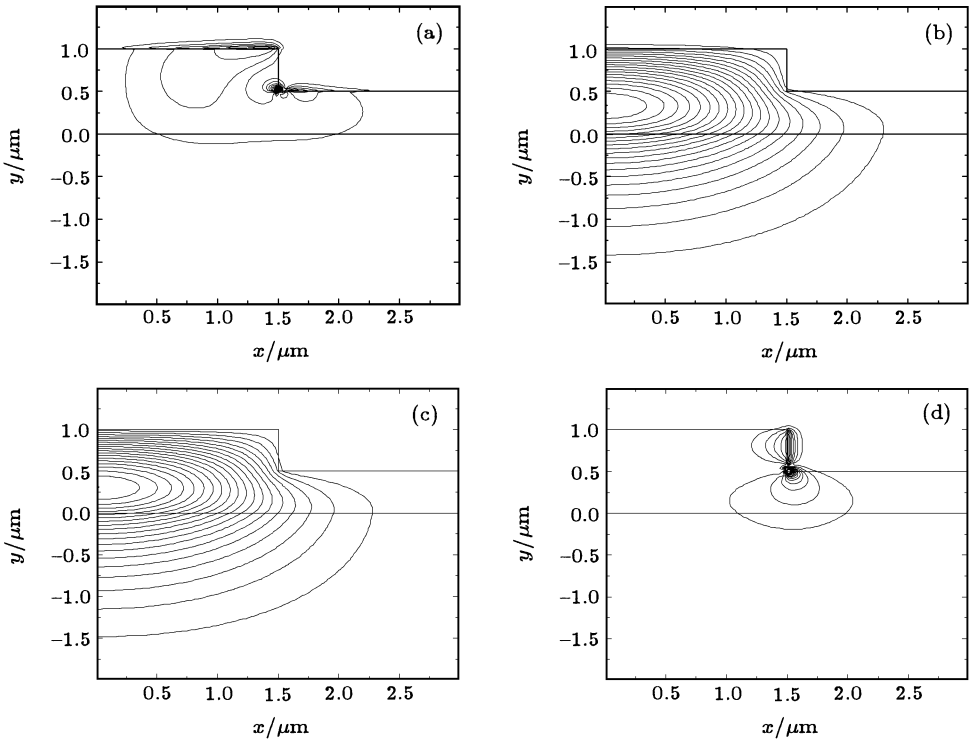


Fig.7. Field patterns of the fundamental mode for a rib waveguide: quasi-TE mode (a) h_x and (b) h_y; quasi-TM mode (c) h_x and (d) h_y.

NTRM[19] are also included in this table. Our results are in excellent agreement with the values from the NTRM, which shows that the present scheme for the CCTs greatly improve the computational accuracy. Figure 7 plots field patterns of the fundamental mode in quasi-TE and quasi-TM modes. Half of the profiles are displayed because of the symmetric structure with respect to x=0. Here again the hybrid nature of the full-vectorial guided-modes is clearly evident.

4. Conclusions

In discretizing the formulation for a 3D-FV-BPM based on H fields along the longitudinal direction, a modified ADI algorithm is proposed. An improved six-point FD scheme is also constructed to approximate the CCTs along the transverse directions. The validity and utility of the present method is assessed by the corresponding imaginary-distance procedure. The field patterns and the normalized propagation constants of the fundamental mode for a buried rectangular waveguide and a rib waveguide are presented. Results show that the present method is efficient and stable, and greatly improve the computational accuracy. In addition, the hybrid nature of the full-vectorial guided-modes is successfully demonstrated. We remark that the present method is a good candidate for analysis, modelling and design of photonic devices and optical waveguides in photonic integrated circuits.

References

[1] Hoekstra H J W M 1997 *Opt. Quantum Electron.* **29** 157

[2] Scarmozzino R, Gopinath A, Pregla R and Helfert S 2000 *IEEE J. Sel. Top. Quantum Electron.* **6** 150

[3] Feng X H, Liu Y G, Sun L, Yuan S Z, Kai G Y and Dong X Y 2005 *Chin. Phys.* **14** 779

[4] Xiao J B, Ma C F, Zhang M D and Sun X H 2006 *Acta Phys. Sin.* **55** 254 (in Chinese)

[5] Lee PC, Schulz D and Voges E 1992 *J. Lightwave Technol.* **10** 1832

[6] Xiao J B, Sun X H and Zhang M D 2004 *Sci. Chin. Ser.* F **47** 34

[7] Dai D X and He S L 2004 *J. Opt. Soc. Am.* A **21** 113

[8] Dai D X and He S L 2004 *Appl. Opt.* **43** 1156

[9] Huang W P and Xu L 1993 *IEEE J. Quantum Electron.* **29** 2639

[10] Hseuh Y L, Yang M C and Chang H C 1999 *J. Lightwave Technol.* **17** 2389

[11] Yamauchi J, Mugita T and Nakano H 2005 *J. Lightwave Technol.* **23** 1947

[12] Press W H, Teukolsky S A, Vetterling W T and Flannery B P 1992 *Numerical Recipes in C-The Art of Scientific Computing* 2nd ed (New York: Cambridge University Press) p827

[13] Yamauchi J, Ando T and Nakano H 1991 *Electron. Lett.* **27** 1663

[14] Liu P L and Li B J 1992 *IEEE J. Quantum Electron.* **28** 778

[15] Rao H 2002 *Optical Electromagnetics Simulation of Strongly Reflective Structures for Integrated Photonics* (New York: Columbia University Press) p181

[16] Jungling S and Chen J C 1994 *IEEE J. Quantum Electron.* **30** 2098

[17] Chamorro-Posada P 2003 *J. Lightwave Technol.* **21** 862

[18] Hadley G R 1992 *IEEE J. Quantum Electron.* **28** 363

[19] Vassallo C 1997 *Opt. Quantum Electron.* **29** 95

[20] Xu C L, Huang W P, Stern M S and Chaudhuri S K 1994 *IEE Proc. Optoelectron.* **141** 281

[21] Xiao J B, Zhang M D and Sun X H 2004 *J. Opt. Soc. Am.* B **21** 798